RSC Advances

Targeted multifunctional tannic acid nanoparticles†

J. R. Aguilera,‡[a] V. Venegas,‡[ab] J. M. Oliva,[a] M. J. Sayagués,[c] M. de Miguel,[d] J. A. Sánchez-Alcázar,[ae] M. Arévalo-Rodríguez[f] and A. P. Zaderenko*[a]

Tannic acid (TA) has multiple effects against cancer, being especially promising in those types that overexpress the epidermal growth factor receptor (EGFR), as TA modulates its activation and downstream signaling pathways, triggering apoptosis. Nonetheless, despite the important role of this receptor in the pathogenesis and progression of a wide variety of tumors, no TA systems targeted to this receptor have been described yet. In this work, we synthesize, characterize by physico-chemical techniques and study the cytotoxic effect and cell uptake of TA nanoparticles targeted to EGFR in both tumoral and normal human skin cells. Our nanoparticles exhibited an extremely high entrapment efficiency, and were only toxic for the tumoral cells. The uptake assay demonstrated that nanoparticles are able to enter the cells through a receptor-mediated mechanism. Furthermore, we have included fluorescent markers in these nanoparticles to combine imaging and therapeutic applications, thus building effectively a multifunctional tool for biomedicine.

Introduction

Tannic acid (TA) is a natural product belonging to the family of tannins, a subset of secondary metabolites known as polyphenols that are widely distributed in the plant kingdom. TA has been shown to exert a wide variety of biological activities including anticancer,[1,2] antioxidant,[3–5] antimicrobial and antiviral activities,[6,7] as well as pro-longevity and a protective effect against several damages and diseases.[8–14]

From a chemical point of view, when compared to other tannins, TA stands out due to its huge number of phenolic hydroxyl groups (Fig. 1). These groups, besides being related to TA biological behavior, make the molecule suitable for use in bottom up complex structures through multiple hydrogen bonds. TA associates with neutral or charged polymers in solution and at surfaces, rendering hydrogen-bonded multilayers,[15] microcapsules,[16] microparticles,[17] emulsomes[18] and hollow multilayer shells[19] which are able to encapsulate anticancer drugs.[20] The formulation of most of these structures involves complex layer-by-layer assembly methods with a sacrificial template. This implies, however, lengthy multi-step syntheses.

From a biological point of view, TA is a complex molecule with a dual behavior; on the one hand, TA is a radical scavenger and hence, a chemopreventive agent, on the other hand, it is also able to induce oxidative stress under certain conditions.[21,22] Therefore, TA exhibits anticarcinogenic[23–26] properties as well as pro-apoptotic activity through the generation of reactive oxygen species (ROS) and the activation of intrinsic apoptotic
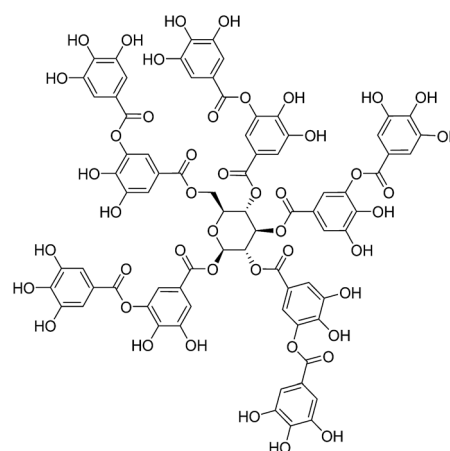
[a]*Departamento de Sistemas Físicos, Químicos y Naturales, Universidad Pablo de Olavide, ES-41013-Seville, Spain. E-mail: apzadpar@upo.es; Fax: +34 954 977305; Tel: +34 954 977365*

[b]*Centro de Investigación Cooperativa en Biociencias, ES-48160-Bizkaia, Spain*

[c]*Instituto de Ciencia de Materiales de Sevilla, ES-41092-Seville, Spain*

[d]*Departamento de Citología e Histología Normal y Patológica, Universidad de Sevilla, ES-41009-Seville, Spain*

[e]*Centro Andaluz de Biología del Desarrollo, ES-41013-Seville, Spain*

[f]*Biomedal S.L, ES-41092-Seville, Spain*

† Electronic supplementary information (ESI) available: Expression of EGFR in HDF and A431 cells (WB); MTT under uptake assay conditions. See DOI: 10.1039/c5ra19405a

‡ J. R. A. and V. V. contributed equally to this work.

Fig. 1 Chemical structure of tannic acid.

pathways.[27–29] Recently, TA crosslinked microparticles have been described to be as effective as cisplatin against A549 cancerous cells, while being much more biocompatible against L929 fibroblast cells.[2] However, their micrometer size limits their biomedical applications. Furthermore, the potential of TA in antitumor therapy is not limited to the induction of apoptosis; and recent studies point out that TA could be used as an adjuvant in cancer therapies since it is also capable of acting as chemosensitizer,[30,31] while reducing resistance to chemotherapeutic drugs by inhibiting detoxification enzymes involved in their clearance.[32] All in all, this complex behavior of TA and dependence on the conditions generates uncertainties as to toxic and/or side effects in some organs or patients at the doses required for chemotherapy.

Another important feature of TA in cancer therapy is that its activity has been associated with receptors that control unwanted proliferation of cells. Recent insights demonstrate that estrogen receptor-positive breast cancer cells are more sensitive to TA-induced apoptosis than triple-negative breast cancer cells and normal breast epithelial cells.[33,34] Moreover, TA modulates the epidermal growth factor receptor (EGFR) activation and its downstream signaling pathways.[35] EGFR is a transmembrane glycoprotein with tyrosine kinase activity involved in regulating cellular proliferation, differentiation, and survival that plays an important role in the pathogenesis and progression of a wide variety of tumors, including gliomas and carcinomas of the lung, colon, head and neck, pancreas, ovary, breast, bladder, and kidney. Thus, EGFR has become a major target in cancer therapy, both in terms of specific inhibition[36–38] and vectorization.[39] Nevertheless, despite the obvious benefits provided by delivering TA to EGFR, no specific delivery system that targets TA to this receptor has been proposed yet.

In the present work we report the preparation of TA nanoparticles targeted to EGFR. We were committed to avoid the use of organic solvents and our system was designed to prevent nonspecific cellular uptake. To this end we self-assembled TA to poly(vinyl alcohol). An additional layer of complexity was introduced in the nanoparticles by encapsulating water-soluble fluorescent markers, giving access to imaging and therapeutic applications. A comparative of uptake and cytotoxicity of targeted and non-targeted TA nanoparticles was performed on human squamous carcinoma cell cultures, which expresses high levels of EGFR, and human dermal fibroblast cell cultures, as control. Our targeted nanoparticles successfully induced cell death in cell cultures overexpressing EGFR.

Results and discussion

Synthesis and characterization of tannic acid nanoparticles

We have developed a method that allowed production of stable tannic acid nanoparticles (TAN) in a single step. These nanoparticles were then coated with a polymer and a protein that enable conjugation to an antibody to EGFR, rendering targeted-tannic acid nanoparticles (Fig. 2).

As mentioned above, TA conjugates to suitable polymers in solution *via* hydrogen bonding. The choice of polymer is critical because its nature will influence the physico-chemical and biological properties of the resulting formulation. Taking this into account, we have chosen poly(vinyl alcohol), PVA, as partner polymer: besides the fact that PVA has multiple hydroxyl groups available for hydrogen bonding with TA, the

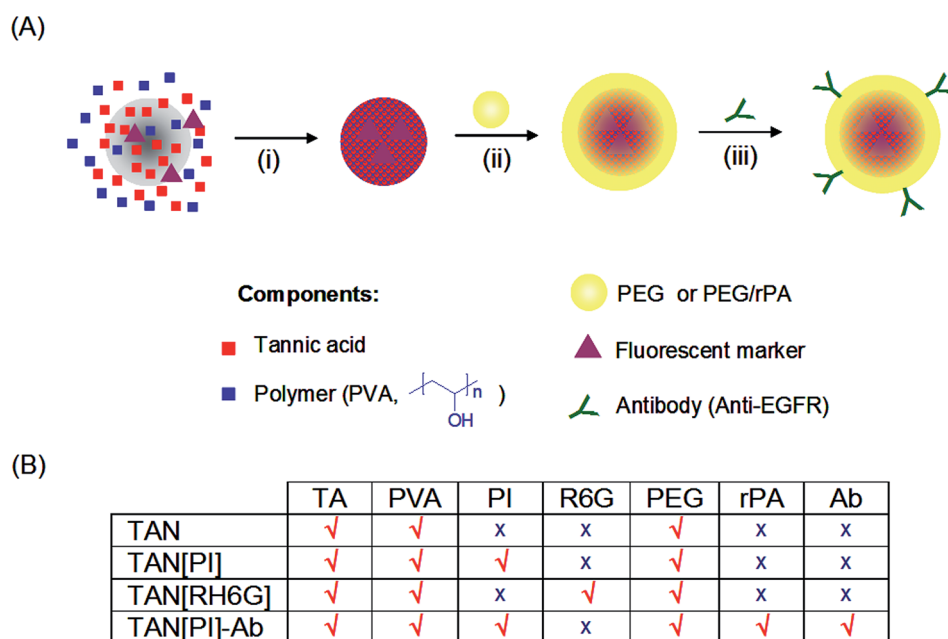|	TA	PVA	PI	R6G	PEG	rPA	Ab
TAN	√	√	x	x	√	x	x
TAN[PI]	√	√	√	x	√	x	x
TAN[RH6G]	√	√	x	√	√	x	x
TAN[PI]-Ab	√	√	√	x	√	√	√

Fig. 2   (A) Schematic representation of nanoparticle fabrication. Synthesis of TA nanoparticles (i). In this step the addition to the reaction medium of a fluorescent marker (optional) allows the fabrication of fluorescent-TA nanoparticles. Nanoparticles were then coated with PEG, or a mixture of PEG and rProtein A (ii) to allow the conjugation to a targeting antibody (iii). (B) Composition of nanoparticles used in this study.

presence of PVA in nanoparticle formulations has been described to affect their cellular uptake, so that nanoparticles with higher amounts of PVA had relatively lower cellular uptake,[40] probably due to the polymer's hydrophilicity. We hypothesize that this must be advantageous because it severely limits unspecific uptake.

Tannic acid nanoparticles were prepared from the respective aqueous solutions of TA and PVA. Upon mixture of the two solutions instantaneous self-assembly of the reagents occurs through hydrogen bonding, leading to the formation of an opalescent off-white suspension of nanoparticles that was dialyzed to remove excess reagents. During the synthesis process, the TA/PVA molar ratio was optimized to maximize TA entrapment efficiency (EE), calculated according to eqn (1) (see Experimental section). The nanoparticles thus obtained achieved a remarkably high EE, $92.2 \pm 0.2\%$, which is very unusual and makes our synthesis very effective and compliant with green chemistry principles.

The physicochemical characterization of nanoparticles showed that they are spherical (Fig. 3A) with a hydrodynamic diameter of 211 nm (Fig. 3B) and a zeta potential of -21 mV. The negative value of the zeta potential is consistent with the presence of negatively charged hydroxyl groups in the nanoparticles stemming from tannic acid, and retains its value after coating with neutral polymers, as we will discuss later on.

The presence of both components, TA and PVA, in the nanoparticles was confirmed by FTIR. Since the interaction between TA and PVA is non-covalent and no chemical change occurs, no major differences are expected in the spectrum of tannic acid nanoparticles and bands of precursors remain, although shifted. Fig. 3C shows the comparison between the FTIR spectra of PVA, TA and tannic acid nanoparticles. In the spectrum of tannic acid nanoparticles, bands of both PVA and TA are observed. The characteristic vibration of the phenol group in TA at 1202 cm^{-1} (νC–O) remains almost unchanged in

tannic acid nanoparticles, and the characteristic band of the aromatic system of TA at 1613 cm^{-1} (νC=C) is shifted to 1606 cm^{-1} in tannic acid nanoparticles. On the one hand, the characteristic vibration of the secondary hydroxyl groups in PVA at 1252 cm^{-1} (νC–O) is shifted to 1258 cm^{-1} in tannic acid nanoparticles, on the other hand, the band located around 3100–3600 cm^{-1} becomes broader, indicating an increased number of hydrogen bonds. Other bands which are affected by the interaction TA–PVA are those due to the ester groups of TA, 1713 cm^{-1} (νC=O), 1320 cm^{-1} (ν_sC–O) and 1029 cm^{-1} (ν_{as}C–O), which are shifted to 1718 cm^{-1}, 1326 cm^{-1} and 1034 cm^{-1} in tannic acid nanoparticles, respectively. These bands, however, overlap with those for the PVA due to the nature of this polymer, which is partially hydrolyzed, and exhibit therefore bands characteristic of esters, as can be seen in the spectrum of the pure compound.

As the ultimate goal of our synthesis is to develop nanoparticles targeted to EGFR, we seek to attach the targeting antibody in the proper orientation that ensures its interaction with the receptor. For this purpose, following the synthesis of tannic acid nanoparticles and according to the strategy shown in Fig. 2A, our nanoparticles were coated with polyethylene glycol (PEG), yielding TAN nanoparticles, which will be further coated with a recombinant protein A (rPA) bearing a PEG-binding domain that enables binding the antibody in a suitable orientation.

PEGylation is an extensively employed technique to produce nanoparticles for biomedical applications given that it camouflages them from opsonins,[41] prevents protein adsorption, nonspecific uptake by cultured cells[42–44] and, moreover, PEGylated nanoparticles can then be functionalized on their surface with the desired molecules or biomolecules.[45,46] A further role of PEG that has been described recently is its use as template during the synthesis of inorganic nanoparticles, with the convenient effect of impairing their non-specific cell uptake.[47]
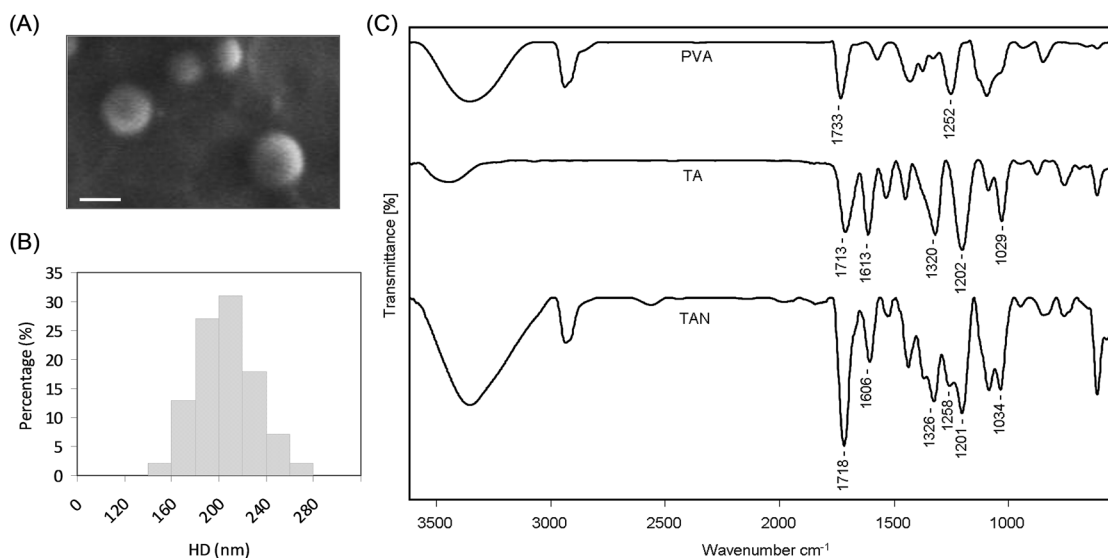

Fig. 3 Tannic acid nanoparticles characterization. (A) SEM image of TA nanoparticles (scale bar 100 nm). (B) Hydrodynamic diameter of TA nanoparticles. (C) FTIR spectra of PVA, TA and TA nanoparticles.

Taking this into account, we have probed two different PEG polymers as coating agents, PEG-bis(amine)-terminated and PEG dihydroxy-terminated. Nevertheless, the PEG-bis(amine)-terminated polymer destabilized the nanoparticles, as a result of the positive charge of the amine groups at physiological pH shielding the negative charge of the NPs. This shows that in this case steric stabilization is insufficient to compensate for the loss of charge. On the other hand, the neutral dihydroxy-terminated PEG does not compromise the stability of the nanoparticles. In this case, the nanoparticles retain their negative charge, as confirmed by a zeta potential of −23 mV, and are further stabilized by steric hindrance. The zeta potential value obtained is within the range of zeta potentials desirable for ensuring stability of colloidal systems stabilized by combined electrostatic and steric interactions.[48] The hydrodynamic diameter of the nanoparticles once coated with PEG increases by around 330 nm, in keeping with twice the chain length of PEG. The fact that the zeta potential is identical to that of the naked nanoparticles, together with the absence of flocculation, suggest that the increase in size is only due to the higher molecular weight of the polymer.[49] Additionally, it has been recently found that it is the core size instead of the total size that is responsible for the homogeneous distribution of PEG coated nanoparticles in the bloodstream and organs within *in vivo* systems.[50]

The FTIR spectrum of PEGylated nanoparticles is otherwise identical to the non-PEGylated one, except for two new and intense bands, characteristic of PEG that appear at 2885 cm^{-1} (νCH_2) and 1112 cm^{-1} (νC–O–C).

Prior to the functionalization of nanoparticles with the targeting antibody, a set of nanoparticles was labeled with a water-soluble fluorescent marker, namely propidium iodide (PI) or rhodamine 6G (R6G), as described in Experimental section to obtain TAN[PI] and TAN[R6G], respectively. Remarkably, the EE was not affected by the addition of fluorescent markers to the reaction medium during the synthesis process, and therefore the labeled nanoparticles obtained showed identical EE than the unlabeled ones (92%).

Propidium iodide (PI) was chosen as fluorescent marker given that the singular features of this compound provides significant benefits when used to investigate cellular uptake of nanoparticles. On the one hand PI is not able to cross intact cell membranes itself and, on the other hand, PI exhibits a weak fluorescence emission that reveals itself only when it binds to DNA or RNA by intercalating between the bases.

Increasing amounts of PI were added in the synthesis media to determine the loading capacity. The loading capacity of nanoparticles, calculated according to eqn (2) (see Experimental section), was found to be 0.3%. It is noteworthy that our loading capacity is 400 times higher than that described for the same marker (PI) in silica nanoparticles, in which labeling capacity in cell cultures had been demonstrated.[51] Moreover, the loading capacity of our nanoparticles is of the same order than that obtained for optimized polyalkylcyanoacrylate nanoparticles.[52] The loading capacity of the other water-soluble fluorescent marker included in this study, R6G, was of similar magnitude at 0.4%. The interest of R6G lies in the fact that this fluorescent

dye is widely used in biological applications to stain mitochondria in living cells.

Both fluorescent nanoparticles, TAN[PI] and TAN[R6G], retained the same zeta potential as unlabeled ones. This can be explained by the fact that the polymer coating of the nanoparticles is electrostatically neutral, whereas the negative charge arises from tannic acid. Nevertheless, labeling with PI causes an increase in particle size of about 10%, while labeling with R6G decreases particle size by about 20%.

Surprisingly, neither PI- nor R6G-loaded nanoparticles released the marker over at least five days, as was found from their release profile in the usual conditions of these assays, *i.e.*, dialysis against different media, including water, phosphate-buffered saline and cell culture medium, and nor was TA released. Within the cell however, the cargo got released as will be shown in the uptake assay on the next pages.

At this stage, nanoparticles were coated with rPA, and conjugated to the antibody, as described in the Experimental section. It should be noted that protein A specifically interacts with the Fc-part of antibodies that belongs to the class of immunoglobulins G (IgG), such as our antibody. With this interaction established, the "paratope" of the antibody remains free and properly oriented to interact with the receptor.[53] The use of this strategy to bind antibodies in an oriented manner has been reported in the field of sensors,[54,55] but to the best of our knowledge is innovative in the field of therapeutic applications.

Cellular cytotoxicity

To assess the cellular cytotoxicity of the nanoparticles, human squamous carcinoma (A-431) and human dermal fibroblast (HDF) cell lines were used. A-431 is an epidermoid carcinoma cell line widely used as model target to study the effect of therapeutic approaches directed to EGFR, owing to its high
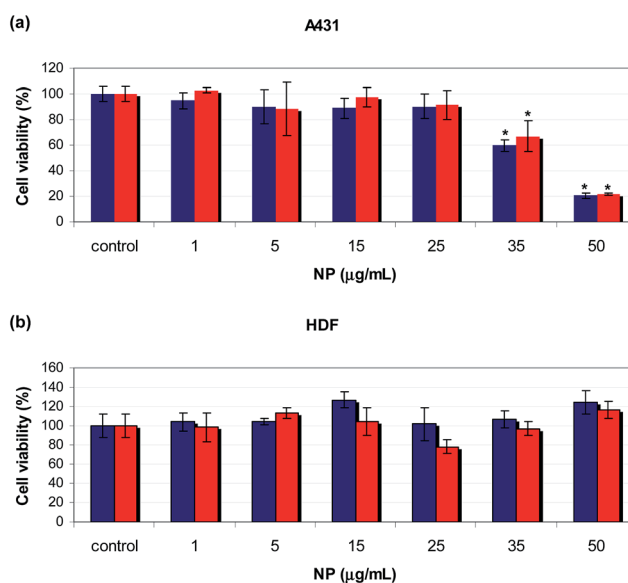

Fig. 4 Cytotoxicity of TAN (blue bars) and TAN[PI] (red bars) on (a) A431 and (b) HDF cells. $n = 5$, *$p < 0.001$.
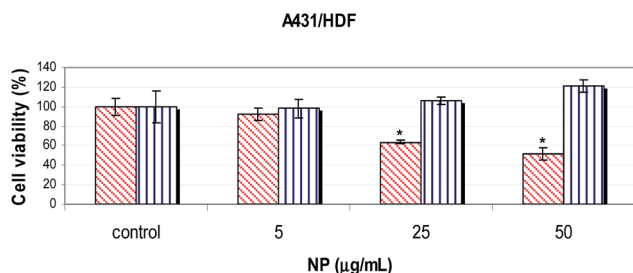
A431/HDF

Fig. 5 Dose-dependent cytotoxicity of TAN-Ab nanoparticles in A-431 (red lines) and HDF (blue lines). $n = 3$. *$P < 0.05$.

EGFR expression, while HDF is derived from the dermis of normal human skin, and its level of expression of EGFR is negligible when compared to A-431.[56] We have assessed the expression of EGFR in both A-431 and HDF by Western blot analysis (Fig. S1, ESI†). The difference in EGFR-expression levels between A-431 and HDF enables them to work as good models for this study.

Given that the uptake assay requires the use of the PI-labeled nanoparticles TAN[PI], their cytotoxicity has been compared with the one of TAN nanoparticles. Cytotoxic activity was evaluated by MTT assay following 48 h exposure to the nanoparticles in concentrations ranging from 1 μg mL^{-1} to 50 μg mL^{-1}. Experimental median toxic dose (TD50) values of TAN and TAN[PI] nanoparticles grown on A-431 cells were found to be 38 ± 1 μg mL^{-1} and 39 ± 1 μg mL^{-1}, respectively (Fig. 4a), while no significant cytotoxicity was found in HDF cells in the assayed range (Fig. 4b). These results are in agreement with the different expression levels of EGFR in both cell lines, A-431 and HDF, and the ability of TA to modulate EGFR activation and downstream signaling.[35]
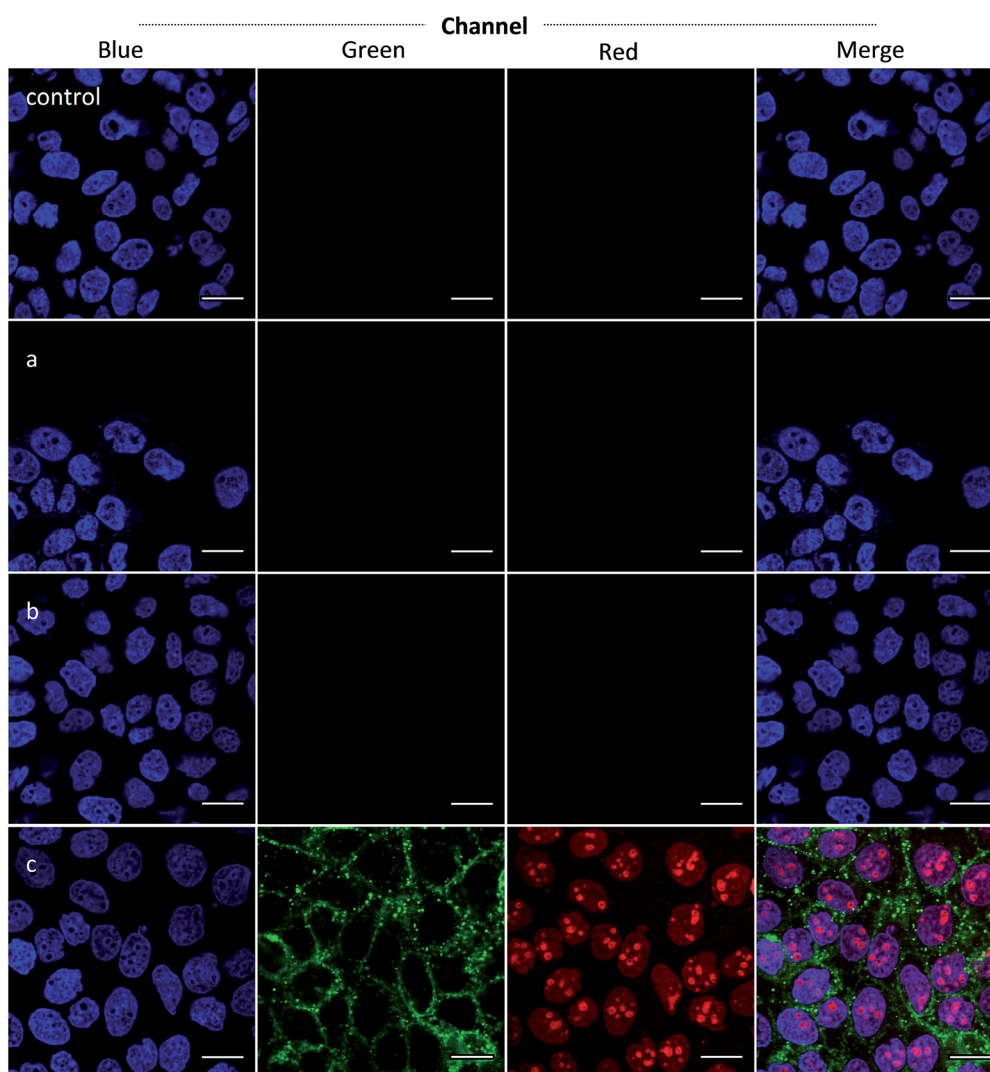

Fig. 6 Fluorescence microscopy images of (from top to bottom): A431 cell cultures (control), A431 cell cultures inoculated with propidium iodide (a), PI-labeled TA nanoparticles (TAN[PI]) (b) and PI-labeled TA nanoparticles conjugated to anti-EGFR (TAN[PI]-Ab) (c). From left to right: blue, green, red and merge channels. Nuclei were stained with Hoechst (blue staining), monoclonal antibody was stained with AF488 (green staining), PI (red staining). Scale bar 25 μm.

The contribution of the fluorescent marker, PI, to the cytotoxic activity of the nanoparticles was found to be negligible.

In the case of the antibody-conjugated nanoparticles (TAN-Ab) grown on A-431 cells, the experimental TD50 values were found to be 10 μg mL^{-1} (25%) higher than those obtained for TAN and TAN[PI] but, interestingly, the deleterious effect resulted to be significant at lower doses (Fig. 5). This decrease in the dose at which cytotoxicity is observed makes sense as the antibody favors the cell uptake, while the increased TD50 might be due to a retarded liberation of the TA from the nanoparticles due to the additional coating of the rPA and antibody.

In HDF cells, no significant cytotoxicity was found in the assayed range (Fig. 5). Overall, the results for A431 and HDF cells are fully consistent with prior findings in the literature for other cell lines, indicating that TA modulates the EGFR activation and its downstream signaling pathways.[35]

Cellular uptake of PI-labeled tannic acid nanoparticles

To further investigate the receptor-specific uptake of our nanoparticles, A-431 cells were incubated with PI-labeled nanoparticles conjugated to a monoclonal antibody to EGFR (TAN[PI]-Ab), as well as with the corresponding nanoparticles without antibody (TAN[PI]) and free PI in solution or nothing at all as control. As mentioned above, labeling nanoparticles with PI does not affect their TA-entrapment efficiency and, since this marker does not cross intact cell membranes and its fluorescence becomes appreciable only after the molecule intercalates between the bases of DNA or RNA, it is suitable to investigate the cellular uptake of nanoparticles by fluorescence microscopy. Therefore, a set of confluent cultures of A-431 cells were inoculated with nanoparticles or PI and cultured for 4 hours. Afterwards, cellular uptake was analyzed by CLSM. In all experiments the concentration of PI used as control was equivalent to the amount of PI in PI-labeled nanoparticles, as indicated in the Experimental section.

The concentration of PI-labeled nanoparticles was optimized taking into account the length of the experiment (4 hours) to achieve good contrast by CLSM, while avoiding possible interferences due to cytotoxicity (such as non-specific cellular uptake of PI owing to apoptosis). As a result of such optimization, a higher dose of nanoparticles was used in the uptake assay (300 μg mL^{-1}), when compared to the MTT (up to 50 μg mL^{-1}), which makes sense given that the former takes place in 4 hours while the second is developed over a 48 hours period.

To assess the cell viability at the dose employed in the uptake experiment, an additional cytotoxicity assay (MTT) was conducted in A-431 cell cultures inoculated with PI-labeled TA nanoparticles conjugated to anti-EGFR at the uptake assay concentration and conditions (Fig. S2, ESI†). Our results demonstrate that this short period of time allows targeted nanoparticles to enter the cell and release sufficient amount of PI to provide good contrast by CLSM (as we will discuss later on in Fig. 6c), but the release of the cargo is still insufficient to exert the deleterious effect of TA observed at longer times (Fig. S2, ESI†). These results are consistent with the increase of TD50 observed in targeted nanoparticles (Fig. 5) when compared to

non-targeted ones (Fig. 4a), which indicates that the cargo release is retarded due to the additional coating of nanoparticles with rPA and antibody.

As shown in Fig. 6, neither free PI (Fig. 6a) nor TAN[PI] nanoparticles (Fig. 6b) were able to cross the cell membrane. A series of images at different points along the z-axis (z-stack) exhibited no cellular uptake of PI and TAN[PI] particles. On the contrary, the fluorescence due to TAN[PI]-Ab nanoparticles was clearly observable (Fig. 6c).

The fluorescence of TAN[PI]-Ab nanoparticles stems from two sources, firstly the targeting antibody is labeled with AF488 (green staining), and secondly nanoparticles themselves are labeled with PI (red staining). Additionally, nuclei were stained with Hoechst (blue staining). As shown in Fig. 6c, both the antibody and PI were detected and PI was able to reach the nucleus during the incubation time, as evidenced by the co-localization of blue and red channels.

Conclusions

In summary, multifunctional tannic acid nanoparticles with an extremely high entrapment efficiency of the active principle and targeted to EGFR were prepared. Our synthesis method offers a real and vastly improved alternative to the current techniques, as this protocol not only does not require the use of organic solvents or sacrificial templates, and the counter polymer, PVA, is classified as GRAS ("generally recognized as safe") by the Food and Drug Administration, but additionally provides nanoparticles targeted to the EGFR receptor and it could easily be generalized to other receptors. These nanoparticles were characterized by FTIR, electronic microscopy and dynamic light scattering. The cytotoxicity assay showed that they were not toxic for the non-tumoral HDF cell line whereas they were markedly toxic for the tumoral cell line A431. The uptake assay demonstrated that the nanoparticles are able to enter the cells through a receptor-mediated mechanism. Nanoparticles could be labeled with fluorescent markers, enabling imaging applications. Remarkably, the labeling does not affect the entrapment efficiency of TA.

Experimental

Materials

Tannic acid, poly(vinyl alcohol) (87–90% hydrolyzed, average M_w 30 000–70 000), rhodamine 6G (R6G), propidium iodide (PI) and polyethylene glycol dihydroxy-terminated (PEG; average M_w 20 000) were purchased from Sigma-Aldrich. Anti-EGFR (528) AF488 sc-120 (Ab) was purchased from Santa Cruz Biotechnology. Recombinant protein A (rPA) was supplied by Biomedal. Water was purified using a Milli-Q (18.2 MΩ) reagent-grade water system from Millipore.

Synthesis of tannic acid nanoparticles

Tannic acid nanoparticles (TAN) were obtained by co-precipitation. Briefly, an aqueous solution of PVA (100 mg, 10 mL) was added to an aqueous solution of TA (34 mg, 10 mL).

The mixture, which turned white immediately, was sonicated at room temperature for 15 minutes in an ultrasonic bath. The excess of reactants was eliminated by dialysis against water for 48 hours to obtain a white suspension of nanoparticles with a concentration of 4 mg mL^{-1}. Finally, the nanoparticles were coated with PEG (5% w/v, final concentration) and recovered by centrifugation (4000 rpm, 20 minutes) to achieve 80 mg of TAN as a white solid.

The amount of TA incorporated in nanoparticles during their formulation was determined by an indirect method. The supernatants and washing solutions obtained during the synthesis of nanoparticles were collected and assayed by Folin–Ciocalteu (FC), following the supplier instructions, to determine the amount of TA that was not incorporated in the formulation. The entrapment efficiency (EE, % w/w) was calculated according to eqn (1).

$$EE(\%) = \frac{\text{added TA} - \text{free TA}}{\text{added TA}} \times 100 \quad (1)$$

TAN nanoparticles were labeled with fluorescent markers by adding water-soluble fluorescent markers to the reaction medium during the synthesis of nanoparticles. Two fluorescent markers, PI and RH6G, were incorporated in nanoparticles as model markers. To determine the loading capacity, increasing volumes of an aqueous stock solution of RH6G (10^{-3} M) or PI (10^{-3} M) were added to the reaction mixture during the synthesis of TAN nanoparticles. This yielded the following final preparation method: 10 mL of an aqueous solution of PVA (10 mg mL^{-1}, containing 300 μL or 200 μL of the stock solution of RH6G or PI, respectively) were added to 10 mL of an aqueous solution of TA (3.4 mg mL^{-1}, containing 300 μL or 200 μL of the stock solution of RH6G or PI, respectively) and sonicated in an ultrasonic bath at room temperature for 15 minutes. The obtained nanoparticles (TAN[RH6G] or TAN[PI], respectively) were coated with PEG (5% w/v, final concentration) and recovered by centrifugation (4000 rpm, 20 min) to obtain 80 mg of TAN[RH6G] as a pink solid or 80 mg of TAN[PI] as a reddish solid.

The loading capacity was estimated by an indirect method. The supernatants and washing solutions obtained during the synthesis of TAN[RH6G] and TAN[PI] were collected and assayed by UV-Vis spectroscopy to determine the amount of RH6G or PI that was not loaded. A standard curve of RH6G or PI was prepared under identical conditions, and free compounds in supernatants were determined by measuring their UV-Vis absorbance at 530 (RH6G) or 617 nm (PI). The loading capacity (LC, % w/w) was calculated according to eqn (2).

$$LC(\%) = \frac{\text{weight of marker loaded}}{\text{nanoparticles weight}} \times 100 \quad (2)$$

where the marker is either RH6G or PI.

To obtain PI-labeled tannic acid nanoparticles targeted to EGFR, TAN[PI] nanoparticles were conjugated to a monoclonal antibody to EGFR through protein A-based chemistry for the immobilization of the target antibody in its correct steric orientation. rPA was produced in bacteria as a translational fusion to a choline/PEG-binding domain,[57] to facilitate

attachment to PEG-coated nanoparticles. Briefly, 2 mg of TAN[PI] nanoparticles were resuspended in 1 mL of Milli-Q water and coated with a mixture of PEG (5% w/v, final concentration) and rPA (5% w/v, final concentration). The mixture was incubated for 2 h at room temperature and the resulting coated nanoparticles were recovered by centrifugation (4000 rpm, 10 minutes), washed two times with Milli-Q water and resuspended in 1 mL of Milli-Q water. Coated nanoparticles (1 mL) were then incubated for 2 h at room temperature with 66 μL of anti-EGFR (50 μg mL^{-1}) to achieve TAN[PI]-Ab immuno-nanoparticles.

Physicochemical characterization of nanoparticles

The size and morphology of tannic acid nanoparticles was characterized by SEM, using a Hitachi FEG S-4800 microscope. The chemical features of tannic acid nanoparticles were characterized by Fourier Transform Infrared Spectroscopy (FTIR). FTIR spectra were recorded on a Bruker IFS 66/s spectrometer equipped with a DTS detector. We averaged 150 scans with a scan frequency of 2.5 Hz and 3 cm^{-1} resolution. The samples were prepared by depositing 100 μL of an aqueous suspension of nanoparticles on a silicon plate. The as prepared samples were allowed to dry at room temperature before recording the spectra. Hydrodynamic diameter, polydispersity index and zeta potential were determined by dynamic light scattering (DLS), using a Zetatrac Analyzer (Microtrac, USA). Measurements were carried out at 25 °C, by placing two milliliters of the nanoparticle suspension in the sample holder.

Cellular cytotoxicity

Two cell lines were used to evaluate the biological behavior of nanoparticles, human squamous carcinoma cell line (A431) and Human Dermal Fibroblast (HDF). Cells were cultured in RPMI medium supplemented with 10% fetal bovine serum (FBS) and 50 U mL^{-1} penicillin per streptomycin, and grown at 37 °C and 5% CO$_2$. Cytotoxicity of TAN nanoparticles was evaluated by MTT assay, according to the kit specifications. The cell viability was expressed as a relative percentage compared to untreated cells. All results are expressed as mean ± standard deviation. The Student's t-test was used to analyse the data and statistically significant differences. Only P-values <0.05 were considered as statistically significant.

Cellular uptake of PI-labeled TA nanoparticles

For PI intracellular release and cell uptake visualization, A431 cells were grown on 1 mm (gold seal no. 1) glass coverslips for 24–48 h in RPMI containing 10% FBS. Stock solutions of TAN[PI], TAN[PI]-Ab and PI were prepared with a PI concentration of 10^{-5} M. Depending on the sample, cells were inoculated with 150 μL of TAN[PI], TAN[PI]-Ab or PI stock solutions and incubated according to Rima et al.[58] with slight modifications. Briefly, inoculated cell cultures were left for 30 min at 4 °C, rinsed twice with PBS and cultured in RPMI medium supplemented with 10% FBS at 37 °C during 4 h. At that stage, cells were rinsed once with PBS, fixed in 3.8% paraformaldehyde for 5 min at room temperature, and permeabilized in 0.1% saponin

for 5 min. Cells were subsequently stained with Hoechst 33342 (1 mg mL^{-1}) and washed with PBS. The presence of PI and anti-EGFR was analyzed by confocal laser scanning microscopy (CLSM) using a Leica SPE Fluorescence Microscope. Lens: 63x oil. Coverslips were mounted onto microscope slides using Vectashield Mounting Medium (Vector Laboratories, Burlingame, CA, USA). LAS AF lite software was used to visualize the uptake effect. Image J software was used for image analysis.

Acknowledgements

References

1 X. Chen, J. a. Beutler, T. G. McCloud, A. Loehfelm, L. Yang, H.-F. Dong, O. Y. Chertov, R. Salcedo, J. J. Oppenheim and O. M. Z. Howard, *Clin. Cancer Res.*, 2003, **9**, 3115–3123.

2 N. Sahiner, S. Sagbas and N. Aktas, *Mater. Sci. Eng., C*, 2015, **49**, 824–834.

3 G. K. B. Lopes, H. M. Schulman and M. Hermes-Lima, *Biochim. Biophys. Acta, Gen. Subj.*, 1999, **1472**, 142–152.

4 R. G. Andrade, J. S. Ginani, G. K. B. Lopes, F. Dutra, A. Alonso and M. Hermes-Lima, *Biochimie*, 2006, **88**, 1287–1296.

5 A. E. Hagerman, K. M. Riedl, G. A. Jones, K. N. Sovik, N. T. Ritchard, P. W. Hartzfeld and T. L. Riechel, *J. Agric. Food Chem.*, 1998, **46**, 1887–1892.

6 P. Buzzini, P. Arapitsas, M. Goretti, E. Branda, B. Turchetti, P. Pinelli, F. Ieri and A. Romani, *Mini-Rev. Med. Chem.*, 2008, **8**, 1179–1187.

7 T. Taguri, T. Tanaka and I. Kouno, *Biol. Pharm. Bull.*, 2004, **27**, 1965–1969.

8 U. R. Kuppusamy and N. P. Das, *Pharmacol. Toxicol.*, 1993, **72**, 290–295.

9 K. T. Chung, T. Y. Wong, C. I. Wei, Y. W. Huang and Y. Lin, *Crit. Rev. Food Sci. Nutr.*, 1998, **38**, 421–464.

10 S. T. Ahmad and S. Sultana, *Hum. Exp. Toxicol.*, 2012, **31**, 145–156.

11 K. Yazawa, T. Kihara, H. Shen, Y. Shimmyo, T. Niidome and H. Sugimoto, *FEBS Lett.*, 2006, **580**, 6623–6628.

12 M. T. Huang, R. L. Chang, A. W. Wood, H. L. Newmark, J. M. Sayer, H. Yagi, D. M. Jerina and A. H. Conney, *Carcinogenesis*, 1985, **6**, 237–242.

13 S. Taffetani, Y. Ueno, F. Meng, J. Venter, H. Francis, S. Glaser, G. Alpini and T. Patel, *Am. J. Pathol.*, 2005, **166**, 1671–1679.

14 I. Perelshtein, E. Ruderman, A. Francesko, M. M. Fernandes, T. Tzanov and A. Gedanken, *Ultrason. Sonochem.*, 2014, **21**, 1916–1920.

15 I. Erel-Unal and S. A. Sukhishvili, *Macromolecules*, 2008, **41**, 3962–3970.

16 T. Shutava, M. Prouty, D. Kommireddy and Y. Lvov, *Macromolecules*, 2005, **38**, 2850–2858.

17 N. Aelenei, M. I. Popa, O. Novac, G. Lisa and L. Balaita, *J. Mater. Sci.: Mater. Med.*, 2009, **20**, 1095–1102.

18 A. Dehsorkhi, V. Castelletto, I. Hamley and P. Harris, *Soft Matter*, 2011, **7**, 10116–10121.

19 V. Kozlovskaya, E. Kharlampieva, I. Drachuk, D. Cheng and V. V. Tsukruk, *Soft Matter*, 2010, **6**, 3596.

20 F. Liu, V. Kozlovskaya, O. Zavgorodnya, C. Martinez-Lopez, S. Catledge and E. Kharlampieva, *Soft Matter*, 2014, **10**, 9237–9247.

21 N. S. Khan, A. Ahmad and S. M. Hadi, *Chem.-Biol. Interact.*, 2000, **125**, 177–189.

22 E. Bouki, V. K. Dimitriadis, M. Kaloyianni and S. Dailianis, *Mar. Environ. Res.*, 2013, **85**, 13–20.

23 F. Majed, S. Rashid, A. Q. Khan, S. Nafees, N. Ali, R. Ali, R. Khan, S. K. Hasan, S. J. Mehdi and S. Sultana, *Mol. Cell. Biochem.*, 2014, **399**, 217–228.

24 O. O. Hamiza, M. U. Rehman, M. Tahir, R. Khan, A. Q. Khan, A. Lateef, F. Ali and S. Sultana, *Asian Pac. J. Cancer Prev.*, 2012, **13**, 4393–4402.

25 M. Katzenellenbogen, L. Mizrahi, O. Pappo, N. Klopstock, D. Olam, H. Barash, E. Domany, E. Galun and D. Goldenberg, *Mol. Cancer Ther.*, 2007, **6**, 1283–1291.

26 C. H. Chen, T. Z. Liu, C. H. Chen, C. H. Wong, C. H. Chen, F. J. Lu and S. C. Chen, *Mol. Nutr. Food Res.*, 2007, **51**, 962–968.

27 Y. C. Chen, L. H. Chien, B. M. Huang and Y. C. Chia, *J. Funct. Foods*, 2014, **7**, 362–372.

28 T.-L. Chang and C.-H. Wang, *Biol. Chem.*, 2013, **394**, 561–575.

29 K. S. Chen, Y. C. Hsiao, D. Y. Kuo, M. C. Chou, S. C. Chu, Y. S. Hsieh and T. H. Lin, *Leuk. Res.*, 2009, **33**, 297–307.

30 Y. Sun, T. Zhang, B. Wang, H. Li and P. Li, *Anticancer Drugs*, 2012, **23**, 979–990.

31 M. Shen, T. Hang Chan and Q. Ping Dou, *Anti-Cancer Agents Med. Chem.*, 2012, **12**, 891–901.

32 P. J. Naus, R. Henson, G. Bleeker, H. Wehbe, F. Meng and T. Patel, *J. Hepatol.*, 2007, **46**, 222–229.

33 B. W. Booth, B. D. Inskeep, H. Shah, J. P. Park, E. J. Hay and K. J. L. Burg, *Int. J. Breast Cancer*, 2013, **2013**, 369609, DOI: 10.1155/2013/369609.

34 T. A. Ngobili, H. Shah, J. P. Y. O. Park, K. W. Kwist, B. Inskeep, K. J. L. Burg and B. W. Booth, *Anticancer Res.*, 2015, **35**, 1285–1290.

35 M. Cichocki, M. Dałek, M. Szamałek and W. Baer-Dubowska, *Nutr. Cancer*, 2013, **66**, 308–314.

36 N. Normanno, A. De Luca, C. Bianco, L. Strizzi, M. Mancino, M. R. Maiello, A. Carotenuto, G. De Feo, F. Caponigro and D. S. Salomon, *Gene*, 2006, **366**, 2–16.

37 J. R. Goffin and K. Zbuk, *Clin. Ther.*, 2013, **35**, 1282–1303.

38 R. Roskoski, *Pharmacol. Res.*, 2014, **79**, 34–74.

39 C. Yewale, D. Baradia, I. Vhora, S. Patil and A. Misra, *Biomaterials*, 2013, **34**, 8690–8707.

40 S. K. Sahoo, J. Panyam, S. Prabha and V. Labhasetwar, *J. Controlled Release*, 2002, **82**, 105–114.

41 D. E. Owens and N. A. Peppas, *Int. J. Pharm.*, 2006, **307**, 93–102.

42 S. Muro, *J. Controlled Release*, 2012, **164**, 125–137.

43 B. Pelaz, P. del Pino, P. Maffre, R. Hartmann, M. Gallego, S. Rivera-Fernández, J. M. de la Fuente, G. U. Nienhaus and W. J. Parak, *ACS Nano*, 2015, **9**, 6996–7008.

44 R. Mout, D. F. Moyano, S. Rana and V. M. Rotello, *Chem. Soc. Rev.*, 2012, **41**, 2539.

45 R. Fernandez-Montesinos, P. M. Castillo, R. Klippstein, E. Gonzalez-Rey, J. A. Mejias, A. P. Zaderenko and D. Pozo, *Nanomedicine*, 2009, **4**, 919–930.

46 P. M. Castillo, M. de la Mata, M. F. Casula, J. A. Sánchez-Alcázar and A. P. Zaderenko, *Beilstein J. Nanotechnol.*, 2014, **5**, 1312–1319.

47 C. Morelli, P. Maris, D. Sisci, E. Perrotta, E. Brunelli, I. Perrotta, M. L. Panno, A. Tagarelli, C. Versace, M. F. Casula, *et al.*, *Nanoscale*, 2011, **3**, 3198–3207.

48 S. Honary and F. Zahir, *Trop. J. Pharm. Res.*, 2013, **12**, 255–264.

49 T. Kotsokechagia, N. M. Zaki, K. Syres, P. de Leonardis, A. Thomas, F. Cellesi and N. Tirelli, *Langmuir*, 2012, **28**, 11490–11501.

50 T. Maldiney, C. Richard, J. Seguin, N. Wattier, M. Bessodes and D. Scherman, *ACS Nano*, 2011, **5**, 854–862.

51 A. Neumeyer, M. Bukowski, M. Veith, C. M. Lehr and N. Daum, *Nanomedicine*, 2011, **7**, 410–419.

52 R. H. Müller, C. Lherm, J. Herbort and P. Couvreur, *Colloid Polym. Sci.*, 1991, **269**, 147–152.

53 A. Kausaite-Minkstimiene, A. Ramanaviciene, J. Kirlyte and A. Ramanavicius, *Anal. Chem.*, 2010, **82**, 6401–6408.

54 J. Neng, M. H. Harpster, H. Zhang, J. O. Mecham, W. C. Wilson and P. A. Johnson, *Biosens. Bioelectron.*, 2010, **26**, 1009–1015.

55 C. C. Lin, Y. M. Yang, Y. F. Chen, T. S. Yang and H. C. Chang, *Biosens. Bioelectron.*, 2008, **24**, 178–183.

56 H. Haigler, J. F. Ash, S. J. Singer and S. Cohen, *Proc. Natl. Acad. Sci. U. S. A.*, 1978, **75**, 3317–3321.

57 B. Maestro, I. Velasco, I. Castillejo, M. Arévalo-Rodríguez, A. Cebolla and J. M. Sanz, *J. Chromatogr. A*, 2008, **1208**, 189–196.

58 W. Rima, L. Sancey, M. T. Aloy, E. Armandy, G. B. Alcantara, T. Epicier, A. Malchère, L. Joly-Pottuz, P. Mowat, F. Lux, O. Tillement, B. Burdin, A. Rivoire, C. Boulé, I. Anselme-Bertrand, J. Pourchez, M. Cottier, S. Roux, C. Rodriguez-Lafrasse and P. Perriat, *Biomaterials*, 2013, **34**, 181–195.